XLI CILAMCE
XLI Ibero-Latin American Congress on Computational Methods in Engineering
16-19 November, 2020 FOZ DO IGUAÇU PARANÁ – BRAZIL

# DEVELOPMENT OF A GUI FOR THE PARAMETRIC STUDY OF MASS FLOW RATES USING THE MATERIAL POINT METHOD

**Lucas Diego de Freitas Lino**
*lucaslino@lccv.ufal.br*
*Undergraduate Student, Center of Technology, Federal University of Alagoas*
**Adeildo Soares Ramos Júnior**
*adramos@lccv.ufal.br*
*Titular Professor, Center of Technology, Federal University of Alagoas*
**Tiago Peixoto da Silva Lôbo**
*tiago@lccv.ufal.br*
*Researcher, Laboratory of Scientific Computing and Visualization*
*Av. Lourival Melo Mota, S/N, Tabuleiro do Martins, 57072-900, Maceió/AL, Brazil*

**Abstract.** Measuring flow rates in engineering applications, whether it's fluid or solid, it's an important task as it often leads to good phenomenon characterization. Particularly, in marine environments, it provides a metric that can be used to safeguard facilities susceptible to landslides. Solving flow rate related problems is a difficult task due to fluid-structure interactions, nonlinearities and phase transitions. Therefore, analytical solutions can be very complex, even impossible to achieve, which usually are the cases approached by geotechnical engineering. Hence, it's preferable to use numerical techniques to solve such problems. In this regard, the material point method is a Lagrangian numerical method where particles move through a background mesh, avoiding distortion problems. This work develops a parametric study of the mass flow rate of a submarine landslide using the software E-Sub, a numerical analysis software developed by the Laboratory of Scientific Computing and Visualization (LCCV). Modelling a submarine landslide often involves many parameters which can dramatically alter the results of the simulation. For this reason, a graphical user interface was developed in which the model is visualized. Furthermore, the interface also allows marking out section planes in which the flow rate is going to be analysed. Lastly, our results showed that the ocean floor plays a major role on all other variables involved in the problem, in which minor changes on its angle lead to bigger changes into flow rates.

**Keywords:** Generalized interpolation material point method, Contact pressure, B-Splines

## 1 Introduction

Submarine landslides are responsible for transporting massive volumes of sediments throughout the seabed and might be the cause of serious damage to submerged structures. Furthermore, it can also be the culprit of civilian causalities, creating tsunamis and other hazards to coastal cities. Numerical modelling of this problem is a difficult task as it involves nonlinearities, interactions between fluid-soil-gas and underwater structures and large deformations, to name a few.

An important measure to comprehend the impact of these large-deformation problems is the mass flow rate as it provides a good understanding of the quantity of energy involved in the sliding process. Analytical computation of the mass flow rate in large-deformation problems is not easily determined as one needed to correctly solve momentum equations for continuous medium. Moreover, we chose the material point method as an alternative to study landslides numerically.

The material point method is an extension of the fluid-implicit-particle (FLIP) method to computational solid dynamics [1]. The MPM is a fully Lagrangian method in which mesh distortion is avoided

and tracking history deformation is possible. By discretizing the continuum into a set of material points that move through a background mesh, where the momentum equation is solved, MPM presents itself as a suitable numerical model to solve large-deformation problems.

In order to determine the mass flow rate we use the material point method and analyze the influence that different geometry or constitutive parameters have on the final result. In conjunction, we also analyze the final distance and peak velocity achieved during the sliding process. Moreover, analyzing the effects of the combination of all parameters involves running numerous assorted simulations. For this purpose, a graphical user interface facilitates the management and control of them.

A graphical user interface is a way of simplify human-machine interaction. Its main purpose is to increase the efficiency and make effortless the use of the corresponding program. Accordingly, to study the effect of changing geometry and soil properties on the mass flow rate, an idealized trapezoidal-based geometry was modelled and through the interface the user can specify the desired side-slops angle, soil slop angle along with the soil height, soil length and the length of the sliding base.

A brief literature review presenting the formulation of the material point method is discussed in section 2. The functionalities of the graphical user interface is presented in section 3. The models created to validate the algorithm to compute the mass flow rate, the choice of parameters used in this study and the results are presented in section 4.

## 2 Material point method

The material point method is a Lagrangian numerical method in which material points move through a background mesh, whereby the equations of motion are resolved [1]. This way, MPM circunvents the mesh distortion problem usually present in Lagragian methods and is accurate to track movements of soils under large deformations [2].

The motion of the continuum is governed by the momentum equation that, using Einstein notation, can be described as:

$$\rho \frac{\partial v_i}{\partial t} = \frac{\partial \sigma_{ij}}{\partial x_j} + \rho b_i \tag{1}$$

in which $v_i$ is the velocity, $\rho(\mathbf{x}_i, t)$ is the density of the continuum body in the current configuration and $b_i$ is the acceleration of gravity.

In this study, the relationship between stress and strain is described with an elastic-plastic model with von Mises yield surface [3–5]:

$$F(\sigma_{ij}) = \overline{\sigma}(\sigma_{ij}) - \sigma_e = \sqrt{3J_2^{'}} - \frac{2}{\sqrt{3}} s_u = 0 \tag{2}$$

where $F(\sigma_{ij})$ is the yield function, $\sigma_{ij}$ is the Cauchy stress tensor and $\overline{\sigma}(\sigma_{ij}) = \sqrt{3J_2^{'}}$ is the effective stress, in which $J_2^{'}$ is the second stress invariant. Plus, $\sigma_e = 2s_u/\sqrt{3}$ is the elastic limit [3], in which $s_u$ is the undrained shear strength.

Equation (1) is the strong form of the conservation of the linear momentum and as the complexity of the problem increases more difficult it is to analytically solve it. Hence, it's established a weak equivalent form of Eq. (1) instead, which takes the form [2]:

$$\int_\Omega \rho \delta u_i a_i d\Omega = \int_{\partial\Omega_t} \rho \delta u_i \tau_i^S dS + \int_\Omega \rho \delta u_i b_i d\Omega - \int_\Omega \rho \frac{\partial(\delta u_i)}{\partial x_j} \sigma_{ij}^S d\Omega \tag{3}$$

in which $\delta u_i$ is the virtual displacement, $a_i = \partial v_i / \partial t$ is the acceleration, $\sigma_{ij}^S = \sigma_{ij}/\rho$ is the specific stress and $\tau_i^S = \tau_i/\rho$ is the specific prescribed surface traction.

In order to solve Eq. (3) we must convert it to a discrete form. MPM uses two different procedures to achieve discretization: represents the continuum in a set of material points and a computational grid in which these points will move through [1, 2, 6]. In this study, an explicit Euler integration scheme along with a lumped (diagonal) mass matrix is adopted since the computational cost per time step is

much lower than that required for an implicit method or the consistent mass matrix [1]. Furthermore, the generalized interpolation material point (GIMP) is also adopted. The discretized momentum equation takes the form:

$$\sum_{l=1}^{n_n} \mathbf{M}_e^i \mathbf{a}_l^i = \mathbf{f}_e^{int,i} + \mathbf{f}_e^{ext,i} \tag{4}$$

in which the superscript *i* denotes the quantities at the time point $t_i$ and $\mathbf{M}_e^i(\mathbf{x}_p^i)$ is the lumped mass matrix evaluated at the position $\mathbf{x}_p^i$ of the material point p, in which $\sum_{p=1}^{n_p}$ is the summation over a finite set ($p = 1, ..., n_p$) of material points with a fixed mass $m_p$, which inside the quantities are evaluated at the material point p. The lumped mass matrix can be calculated using:

$$\mathbf{M}_e^i(\mathbf{x}_p^i) = \sum_{p=1}^{n_p} m_p N_e(\mathbf{x}_p^i); \tag{5}$$

the external forces vector evaluated at the node *e* is given by:

$$\mathbf{f}_e^{ext,i} = \sum_{p=1}^{n_p} m_p \mathbf{b}^i(\mathbf{x}_p^i, t) N_e(\mathbf{x}_p^i); \tag{6}$$

and the internal forces vector can be shown to be:

$$\mathbf{f}_e^{int,i} = -\sum_{p=1}^{n_p} m_p \boldsymbol{\sigma}_p^{S,i}(\mathbf{x}_p^i, t) \cdot \nabla N_e(\mathbf{x}_p^i). \tag{7}$$

$N_e(\mathbf{x}_p^i)$ and $\nabla N_e(\mathbf{x}_p^i)$ are the shape function and its gradient evaluated at the node *e* at the point position $\mathbf{x}_p^i$. Lastly, $\sum_{l=1}^{n_n}$ denotes the summation over the spatial nodes and $n_n$ is the number of mesh nodes.

The numerical computation of the mass flow rate is implemented taking advantage of the discretization of the material point method. The MPM discretizes the material domain with a set of particles (material points with a fixed mass) carrying all necessary information with them (i.e., mass, momentum, energy, strain, stress, and internal state variables for history-dependent constitutive modeling).

In conventional MPM particles have no finite dimensions (as they are described as a Dirac delta), whereas in GIMP particles have a finite volume, but this volume is not tracked and deformed during the simulation. As we are using GIMP in our calculations, we assume that each particle occupy a finite region given by a square centered in the particle position. The size of the square is chosen to be the one that has the volume the particle have during the simulation.

In each step of the simulation, the sliding mass is computed in which is divided in a mass to the right side of the section plane and a mass to the left side of the section plane. Thereby, the variation of the mass of the current time step is computed and divided by the time step, which is small enough to be consistent, leading to the mass flow rate, namely:

$$\dot{m} = \lim_{\Delta t \to 0} \frac{\Delta m}{\Delta t} \tag{8}$$

in which $\dot{m}$ is the mass flow rate, $\Delta m$ is the variation of the mass passing a surface and $\Delta t$ is the variation of time. Equation (8) is general and can take the form:

$$\dot{m} = \rho \cdot \mathbf{v} \cdot \mathbf{A} \tag{9}$$

where **v** is the velocity of the mass and **A** is the section plane vector area that the mass is passing through. The solution of Eq. (11) is only true for a flat plane area and can be used in simple problems as the ones presented to validate the mass flow rate.

## 3 Graphical User Interface

A graphical user interface (GUI) was created to allow better management of numerical simulations. Specifically, the GUI main goal is to facilitate the visualization and modelling of pre-defined problem templates. Moreover, the GUI allows the user to fine tune parameters of the desired template, enabling parametric studies to be performed and tracked in an intuitive fashion. Additionally, one can visualize, modify and create models and parametric studies directly from the GUI.

The main screen of the GUI is shown in Fig. 1. This view addresses the template of a landslide, the one we will use in the rest of this work. Two main elements are shown: the parameters boxes and the simplified view of the template in question.

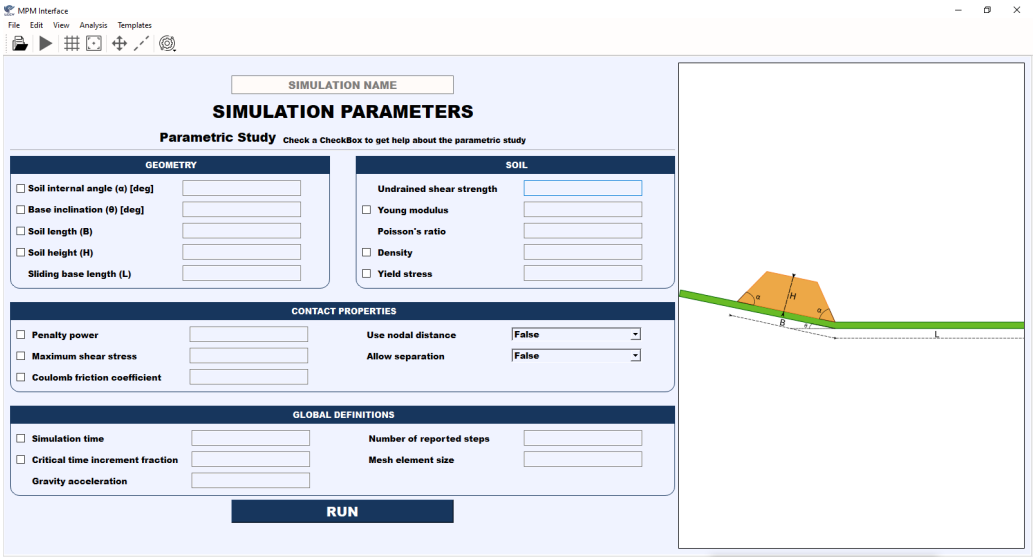


Figure 1. Initial tab that is shown when the GUI is opened

Parametric values can be passed in two different formats: discrete (i.e., *6, 7, 8, 9*) or incremental (i.e., *6 : 1 : 9*), allowing the user to fine tune the parametric analysis. However, not all variables are parametric. Those which can be treated as a parametric value have a check box in the left side of their labels. When checked, a tool button is displayed in the right side of the input space showing the full range of the variable. Another feature of the GUI is the ability to manually insert a plane where flow rates will be measured in the numerical simulation (Fig. 2).

## 4 Results

The analysis module used in this paper to solve the problems was the software E-Sub, developed by the researchers of the LCCV. In this work we added the calculation of flow rates into the software and, because of this, the first example we will show is a verification of this implementation. It is important to add that we are using the contact model described in [7] where a limiting shear stress $\tau_{max}$ is specified along the contact interface to better represent the geotechnical problem.

In order to validate the numerical implementation of the mass flow rate calculation, we simulated a rectangular block sliding on a flat plane. The density of the sliding mass was $\rho = 600kg/m^3$ and a prescribed velocity of $4m/s$ was set to the moving block. A 2x2 particle configuration was used, the critical time increment fraction $\Delta t$ was taken as $0.15s$ and the acceleration of gravity was $10m/s^2$.

The block height and length were taken as $0.3m$ and $1m$, respectively (see Fig. 2). Additionally, a maximum shear stress of $\tau = 0.36kPa$ was specified and a mesh element size of $0.08m$, $0.04m$ and $0.02m$ were chosen to ensure that the implementation is correct. In this case, a deceleration force is acting on the contact area and it can be determined as seen in Eq. (10).

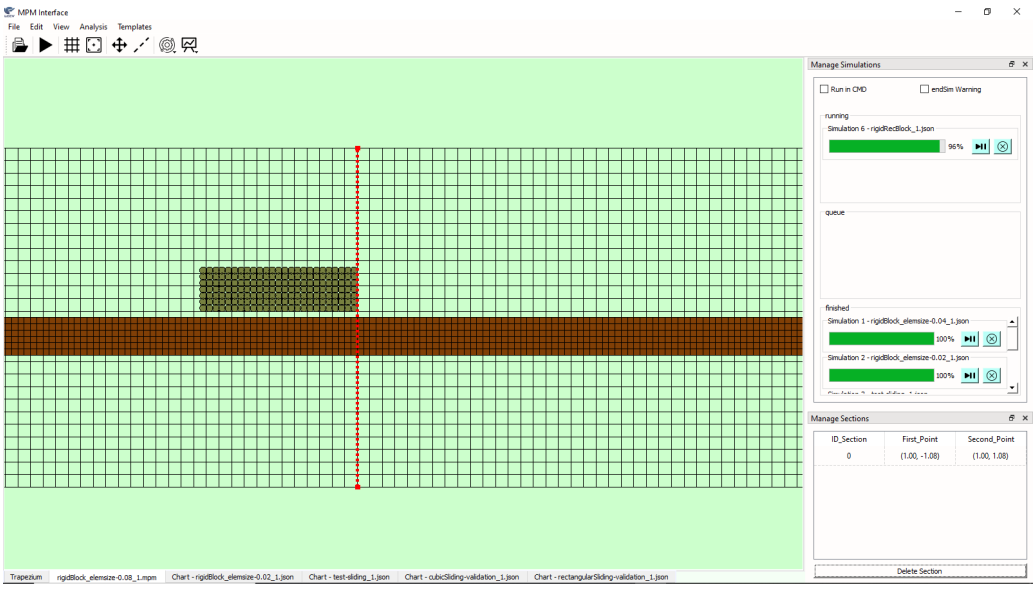


Figure 2. Insertion of a flow rate measure plane depicted in the GUI

$$a = \frac{\tau}{\rho \cdot h} = \frac{360}{600 \cdot 0.3} = 2m/s^2 \tag{10}$$

Considering the initial velocity of $4m/s$ and a deceleration force of $2m/s^2$, the block is expected to slide for $2s$ covering a final distance of $4m$ then stopping. The mass flow rate can be calculated using Eq. (9) as follows:

$$\dot{m} = 600 \cdot 4 \cdot 0.3 = 720kg/s \tag{11}$$

Furthermore, as the mass flow rate is directly proportional to the velocity of the mass, its curve declines with time and it's expected that the block fully passes through the section plane after $0.27s$ with a velocity of $3.46m/s$ thus with the mass flow rate $\dot{m} = 622.8kg/s$. Figure 3a shows the displacement of the center of mass along with its analytical displacement. The final displacement of the center of mass calculated with $0.08m$, $0.04m$ and $0.02m$ mesh element size were $3.91m$, $4m$ and $3.97m$, respectively. The results of all three simulations were close to the theoretical results as expected. Figure 3b shows the mass flow rate chart obtained from the simulation with mesh element size of $0.02m$. As expected, its curve is decreasing from a value of $720kg/s$ to a value of $622.8kg/s$ at $0.27s$ and after, as the block has already passed the section plane, the mass flow rate is null.

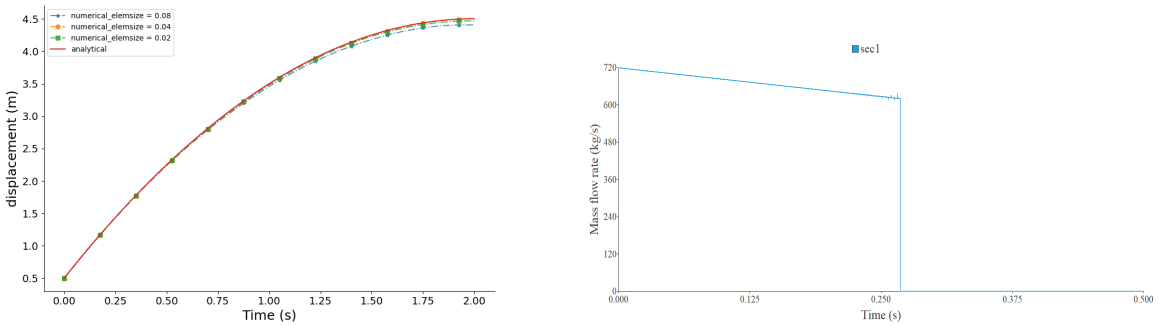


(a) Displacement of the center of mass with different mesh element sizes

(b) Mass flow rate chart from the simulation with mesh element size of $0.02m$

Figure 3. Results of the validation of the mass flow rate

We also tested the flow rate when there is no limiting shear stress being specified in the contact interface. In this model, all parameters were equal to the previous one except that the height, length and mesh element size were taken as $4.5m$, $7.5m$ and $0.1m$, respectively. Since the sliding block has a prescribed velocity of $4m/s$ and no resistance is performed on the contact area, at $1.875s$ it should pass the section plane with the constant value of $\dot{m} = 10800kg/s$ (Fig. 4).

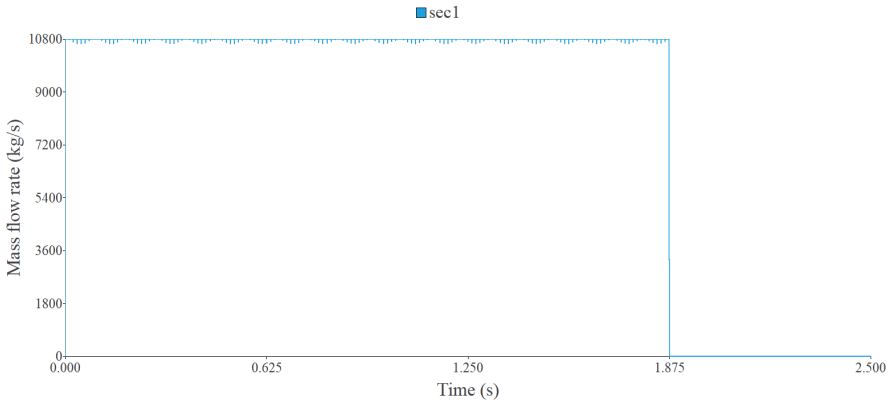


Figure 4. Results of the validation of the mass flow rate of the block with no limiting shear stress

It's notorious some oscillations on the curve of the mass flow rate chart (see Fig. 4) even it should have a constant value. These oscillations are caused due to the finite area approach as discussed in section 2. Since the particles are treated as having a square shape proportional to the volume, small voids between them are bound to happen during simulation, leading to oscillations in the calculation of the mass flux $\dot{m}$.

### 4.1 Parametric Study

To achieve a better understanding of the landslide process we opted to study the problem parametrically. Specifically, we focused on determining the effects that geometry and soil properties could cause on the reach, velocity and flow rate. In all simulations, unless otherwise stated, each cell was initialized with $9$ material points. The acceleration of gravity was $9.81m/s$ and Poisson's ratio was taken as $0.49$ to approximate incompressibility.

We varied the base inclination angle and soil Young's modulus. The angle varied from $2°$ to $5°$ and Young's modulus varied from $50s_u$ to $250s_u$, where $s_u$ is the undrained shear strength of the soil.

The mesh element size was taken as $1m$, which corresponds to approximately $9.1k$ material points and the critical time increment fraction $\Delta t$ was taken as $0.15s$. The submerged density of the sliding mass was taken as $\rho = 600kg/m^3$. Furthermore, for the study of the mass flow rate, we planted one vertical section plane always located at the x position of the right down vertex of the sliding mass, comprehending the vertical limits of the mesh (see Fig. 5).

Should be evident that as the inclination angle of the sliding base increases, higher is the value of the displacement of the front toe. Figure 6a shows a comparison between the displacement of the front toe of the simulations with the same Young's moduli and different base inclination angles.

When the base inclination angle is taken as $\theta = 5°$ the sliding mass achieved a peak front toe velocity of $9.51m/s$ at $2s$ and a final run out distance of $38.8m$. The final front toe displacement of the simulations with $2°, 3°$ and $4°$ were $19.1m, 23.63m$ and $30.48m$, respectively.

The influence of the Young modulus on the displacement of the front toe didn't demonstrate significant effects. Figure 6b shows a comparison between the final run out distances of the simulations with $5^o$ of base inclination and varying their Young's moduli. The final run out distances were very close to each other, presenting a standard deviation of $0.2m$. The minimum distance was $38.63m$ with Young's modulus of $200s_u = 500kPa$ and the maximum was $39.18m$ with Young's modulus of $250s_u = 625kPa$.

The mass flow rate suffered more influence resulting from the base inclination angle. A exponential

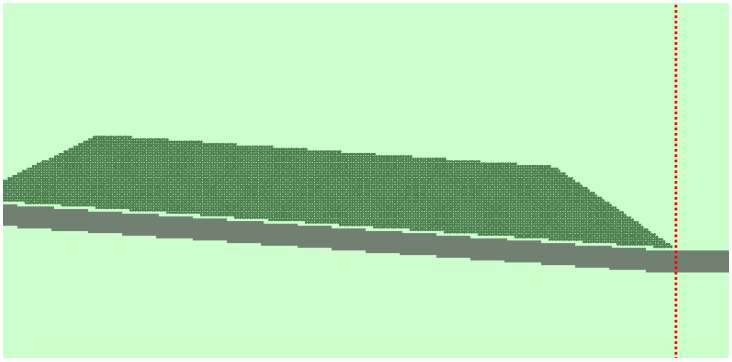

Figure 5. Location of the section planes

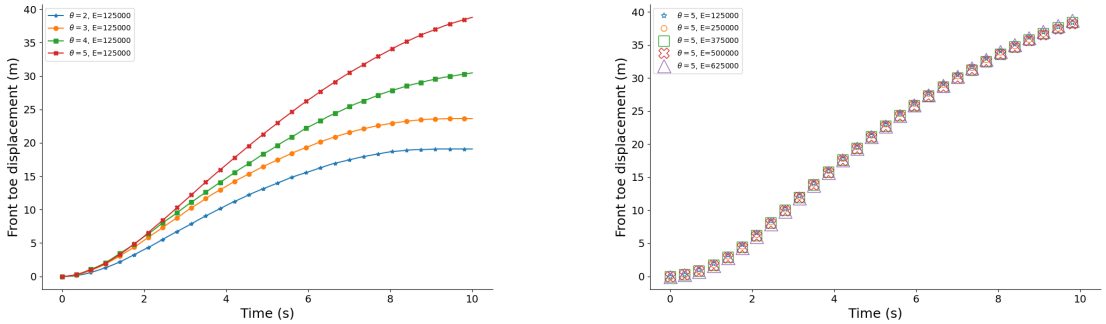


(a) Comparison between the displacement of the front toe of the sliding masses by varying their base inclination $\theta$

(b) Comparison between the displacement of the front toe of the sliding masses with $\theta = 5°$ of base inclination by varying their Young's moduli $E$

Figure 6. Comparison of the final run out distances varying base inclinations ($\theta$) and Young's moduli ($E$)

moving average was performed and is displayed along with the mass flow rate chart due to the great oscillations cause by the voids between the particles that naturally appear during the sliding of the mass. In the first $2.5$ seconds the mass flow rate increases significantly then starts decreasing. The rate of decrease is higher when the base inclination is lower. This means that as the base inclination angle increases, the mass flow rate values are higher during the sliding of the mass. Figure 7 shows the mass flow rate charts of the simulations with Young's moduli of $50s_u$ and $250s_u$ and base inclinations of $2^o$ and $5^o$. It was noticeable a minor decrease in the value of the mass flow rate in relation with simulations with lower Young's modulus to simulations with higher Young's modulus.

Figures 7a to 7d shows the mass flow rate peak of all simulations, which happens close to $2.5s$. The simulations with Young's modulus $E = 50s_u$ and base inclinations $\theta = 2°, 5°$ reached a peak value of $7171kg/s$ and $11408kg/s$, respectively. Those with Young's modulus $E = 250s_u$ and base inclinations $\theta = 2°, 5°$ reached a peak value of $6816kg/s$ and $11387kg/s$, respectively (Fig. 7).

## 5 Conclusions

Submarine landslides transport a vast amount of sediments that might cause great damages to facilities susceptible to them. We analyzed the influence of the seabed slope on the landslide and developed a GUI that facilitates the study. In addition, the numerical computation of the mass flow rate proved to be consistent with analytical results. Furthermore, we observed that the dynamic behavior of the landslide was relatively unchanged for a variation of $500$ KPa of the Young modulus of the soil. Moreover, seabed inclination played a major role on all the variables we observed, where minor changes into this variable caused a way bigger change into flow rates, velocities and displacement of the mobilized soil.

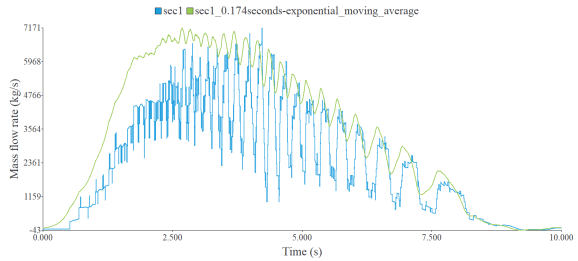


(a) Mass flow rate chart - Young's modulus = $50s_u$ and base inclination = 2°

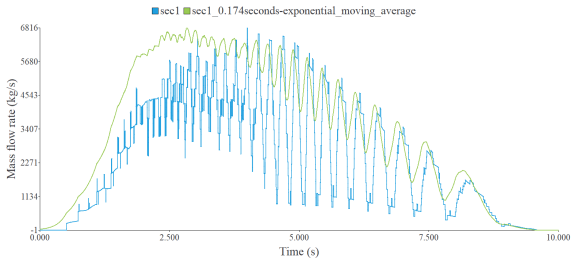


(b) Mass flow rate chart - Young's modulus = $250s_u$ and base inclination = 2°

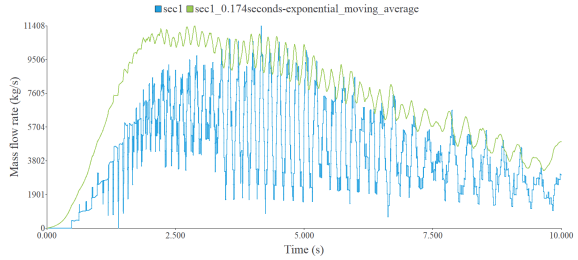


(c) Mass flow rate chart - Young's modulus = $50s_u$ and base inclination = 5°

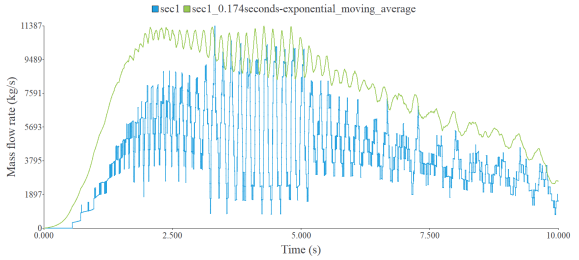


(d) Mass flow rate chart - Young's modulus = $250s_u$ and base inclination = 5°

Figure 7. Results of the mass flow rate of the parametric study

To have a more realistic representation of the soil a constitutive model that accounts for strain softening and rate-dependency is more suitable and it is being considered for future works.

**Authorship statement.** The authors hereby confirm that they are the sole liable persons responsible for the authorship of this work, and that all material that has been herein included as part of the present paper is either the property (and authorship) of the authors, or has the permission of the owners to be included here.

## References

[1] Zhang, X., Chen, Z., & Liu, Y., 2016. *The material point method: a continuum-based particle method for extreme loading cases*. Academic Press.

[2] Dong, Y., 2017. *Runout of submarine landslides and their impact on subsea infrastructure using material point method*. PhD thesis, Ph. D. Thesis, Centre for Offshore Foundation Systems, The University of ....

[3] Oliver, X. & Saracibar, C. A. d., March 2017. Continuum mechanics for engineers. *Theory and problems*.

[4] Shames, I. H. & Cozzarelli, F. A., 1997. *Elastic and inelastic stress analysis*. CRC Press.

[5] Hjelmstad, K. D., 2007. *Fundamentals of structural mechanics*. Springer Science and Business Media, 2nd edition.

[6] MA, J., 2015. Numerical modelling of submarine landslides and their impact to underwater infrastructure using the material point method.

[7] Ma, J., Wang, D., & Randolph, M., 2014. A new contact algorithm in the material point method for geotechnical simulations. *International Journal for Numerical and Analytical Methods in Geomechanics*, vol. 38, n. 11, pp. 1197–1210.